MATERIALS CHEMISTRY FRONTIERS

CCS 中国化学会 CHINESE CHEMICAL SOCIETY

ICCAS

ROYAL SOCIETY OF CHEMISTRY

RESEARCH ARTICLE

View Article Online
View Journal | View Issue

Cite this: *Mater. Chem. Front.*, 2021, **5**, 4997

Alloying Cs^+ into Rb_2ZrCl_6:Te^{4+} toward highly efficient and stable perovskite variants

Jun Zhou, †*[a] Ximing Rong, †[b] Maxim S. Molokeev,[cde] Yulong Wang,[a] Xiangyan Yun,[a] Denghui Xu *[a] and Xiong Li[a]

Received 22nd February 2021,
Accepted 20th April 2021

DOI: 10.1039/d1qm00302j

rsc.li/frontiers-materials

Doping or alloying in perovskites and perovskite variants provides a promising way for modulating the electronic and photoluminescence properties and the structural stability. In this work, a series of yellow-emitting $Rb_{2-x}Cs_xZrCl_6$:Te^{4+} solid solution phosphors were prepared by a hydrothermal method, and their broad emission is assigned to the triplet $^3P_1$–$^1S_0$ self-trapped excitons (STEs). Upon increasing the alloying ion Cs^+, the yellow emission can be greatly enhanced by a stronger Jahn–Teller distortion. Moreover, Cs_2ZrCl_6:Te^{4+} shows a high photoluminescence quantum yield (PLQY), and impressive thermal and anti-water stability. This doping–alloying strategy presents a new direction towards designing lead-free, high-performance and stable perovskite derivatives.

Introduction

Lead halide perovskites with general formula $APbX_3$ (where A = $CH_3NH_3^+$ and $CH(NH_2)_2^+$, and Cs^+; X = Cl^-, Br^-, and I^-) have attracted great interest in many fields such as light emitting diodes, solar cells and photoelectric detectors due to their outstanding optoelectronic and optical properties.[1–4] However, the toxic nature of lead along with thermal and moisture instability further limits commercialization.[5] To solve these issues, various lead-free perovskites are being developed now. Sn(II) and Ge(II) with low toxicity are considered as promising candidates for Pb replacement because they have a similar electronic configuration and the same valence.[6] However, the chemical instability of alternative elements and poor optoelectronic performance give rise to limitations for their practical application.[7] Meanwhile, use of the vacancy-ordered perovskite variants ($A_2B(IV)X_6$) with a 50% B(IV) defect molecular salt structure featuring isolated $[BX_6]^{2-}$ octahedra have become an effective way to solve the above issues due to their excellent stability.[8,9] Nevertheless, a large number of B(IV) vacancies in $A_2B(IV)X_6$ structures affect carrier migration and recombination, leading to extremely low quantum efficiency.[10] Hence, it is of great practical significance to develop an effective method to modify the optoelectronic properties of $A_2B(IV)X_6$ perovskite variants.

Recently, doping or alloying has been demonstrated as an effective method to modulate the structure and photoluminescence properties.[11,12] Bi^{3+}, Sb^{3+}, transition-metal ions (Mn^{2+} and Cu^{2+}), and lanthanide ions (Tb^{3+} and Ce^{3+}) are usually doped as luminescent centers in perovskites and perovskite variants.[13–15] Amongst them, tetravalent tellurium (Te^{4+}) is an important optically active luminescent ion, which has an ionic radius and electronic configuration of $5s^2$ similar to those of Pb^{2+}. Indeed, several articles reported the luminescence of Te^{4+} as a matrix or an activator in $A_2B(IV)X_6$ perovskite variants, and the yellow broad-band emission is caused by a strong Jahn–Teller distortion of the $[TeX_6]^{2-}$ octahedra.[16–19]

In inorganic metal halides, A-site engineering is an important means of changing the optical properties.[20,21] Recently, Zeng *et al.* reported that only a small amount of Rb^+ doping can improve the luminescence intensity of Cs_2ZrCl_6:Te^{4+}, while a large amount of Rb^+ doping will reduce the luminescence intensity. However, the explanation about the influence of Rb^+ on the luminescence properties of Cs_2ZrCl_6:Te^{4+} is very little and vague.[22] To the best of our knowledge, the introduction of alloying A-site ions into Te^{4+}-doping $A_2B(IV)X_6$ perovskite variants, so as to tune the Jahn–Teller distortion of the $[TeX_6]^{2-}$ octahedra and the photoluminescence of Te^{4+}, has not been reported to date. Herein, we fabricated a series of yellow-emitting $Rb_{2-x}Cs_xZrCl_6$:Te^{4+} perovskite variants by a hydrothermal method. Combining the absorption spectra and Stokes shift, the yellow emission of Te^{4+} can be greatly enhanced by a

[a] *Department of Physics, Beijng Technology and Business University, Beijing 100048, China. E-mail: jzhou1204@btbu.edu.cn, xudh@btbu.edu.cn*
[b] *Shenzhen Key Laboratory of Special Functional Materials, Shenzhen Engineering Laboratory for Advanced Technology of Ceramics, Guangdong Research Center for Interfacial Engineering of Functional Materials, College of Materials Science and Engineering, Shenzhen University, Shenzhen 518060, P. R. China*
[c] *Laboratory of Crystal Physics, Kirensky Institute of Physics, SB RAS, Krasnoyarsk 660036, Russia*
[d] *Siberian Federal University, Krasnoyarsk, 660041, Russia*
[e] *Department of Physics, Far Eastern State Transport University, Khabarovsk, 680021, Russia*
† These authors contributed equally.

stronger Jahn–Teller distortion by increasing the alloying ion Cs^+. Moreover, Cs_2ZrCl_6:Te^{4+} has excellent thermal and anti-water stability, which has highly promising prospects in solid state lighting. The design rule established here will provide an efficient way to design luminescent materials with excellent properties.

Experimental

Materials and preparation

$Rb_{2-x}Cs_xZr_{0.9}Cl_6$:$0.1Te^{4+}$ perovskite variants were grown from HCl solution by the hydrothermal method. All the chemicals were commercially purchased and used without further purification. Stoichiometric amounts of raw materials RbCl (99.99%, Aladdin), CsCl (99.99%, Aladdin), $ZrCl_4$ (99.99%, Aladdin), $TeCl_4$ (99.99%, Aladdin) and HCl solution were loaded into a stainless steel Parr autoclave. A yellow powder was precipitated from the solution upon heating at 453 K for 12 h. This obtained $Rb_{2-x}Cs_xZr_{0.9}Cl_6$:$0.1Te^{4+}$ solid was rinsed with ethanol and dried under reduced pressure overnight.

Characterization

The powder X-ray diffraction (XRD) patterns of $Rb_{2-x}Cs_xZr_{0.9}Cl_6$:$0.1Te^{4+}$ samples were examined with a Germanic model D2 PHASER (Bruker, Karlsruhe) using Cu-Kα radiation (λ = 0.1506 Å), which was operated at 30 kV and 10 mA. The powder diffraction pattern for Rietveld analysis was collected with the same diffractometer, but the step size of 2θ was 0.016° and the counting time was 1 s per step. Rietveld refinement was performed by using the TOPAS 4.2 software.[23] The absorption spectra were measured at room temperature using a Varian Cary 5 ultraviolet-visible-near infrared spectrophotometer. The room-temperature excitation (PLE) and room-temperature emission (PL) spectra were recorded using an FS5 fluorescence spectrophotometer (Edinburgh Instruments Ltd, U.K.). The room-temperature decay curves were also recorded on the FS5, and 365 nm pulse laser radiation was used as the excitation source. Wavelength-dependent PLE spectra were recorded using an FLS920 fluorescence spectrophotometer (Edinburgh Instruments Ltd, U.K.). Temperature-dependent PL spectra were measured from 80 to 350 K using the FLS920, low temperature measurements using a liquid nitrogen cryostat on Oxford Instruments attached to the FLS920, and high temperature measurements using a connected heating equipment. The photoluminescence quantum yield (PLQY) was measured using the integrated sphere on the same FLS920 instrument, and white $BaSO_4$ powder was used as a reference to measure the absorption. Thermogravimetric analysis (TGA) was performed on a Setaram Labsys Evo at 10 °C min^{-1} in an argon flow from room temperature to 1000 °C. The Fourier transform infrared spectrum (FT-IR) was recorded on a Thermo Scientific Nicolet iS10.

Results and discussion

Crystal structure

The expected crystal structure and doping mechanism of as-prepared $Rb_{2-x}Cs_xZr_{0.9}Cl_6$:$0.1Te^{4+}$ are presented in Fig. 1a. The isolated $[ZrCl_6]^{2-}$ octahedra and 12-fold coordinated Cs^+/Rb^+ cations are located in the cavities formed between the octahedra, forming a 3-dimensional vacancy-ordered structure. Because Te^{4+} and Zr^{4+} have similar coordination properties with Cl^-, Te^{4+} should occupy the position of Zr^{4+}, so that the strains and lattice defects caused by doping can be suppressed as much as possible.[16] The XRD patterns of the as-synthesized $Rb_{2-x}Cs_xZr_{0.9}Cl_6$:$0.1Te^{4+}$ (x = 0, 0.5, 1.0, 1.5 and 2.0) samples are exhibited in Fig. 1b, together with the standard patterns of Rb_2ZrCl_6 (JCPDS 74-1000) and Cs_2ZrCl_6 (JCPDS 74-1011). All the diffraction peaks are consistent with the standard cubic crystal structure, indicating that Cs^+ and Te^{4+} ions could be successfully incorporated in the host structure. Rietveld refinement was used to further study the effect of Cs^+ on the crystal structure, and the variation of cell volumes of $Rb_{2-x}Cs_xZr_{0.9}Cl_6$:$0.1Te^{4+}$ dependent on x values is given in Fig. 1c. It can be obviously seen that the cell volumes increase linearly, indicating that the bigger Cs^+ substitutes for smaller Rb^+ in the lattice and the formation of an iso-structural solid solution.

Optical properties

Te^{4+} is a typical ion with the outer electronic configuration of $5s^2$ and the splitting of the energy levels can be described as

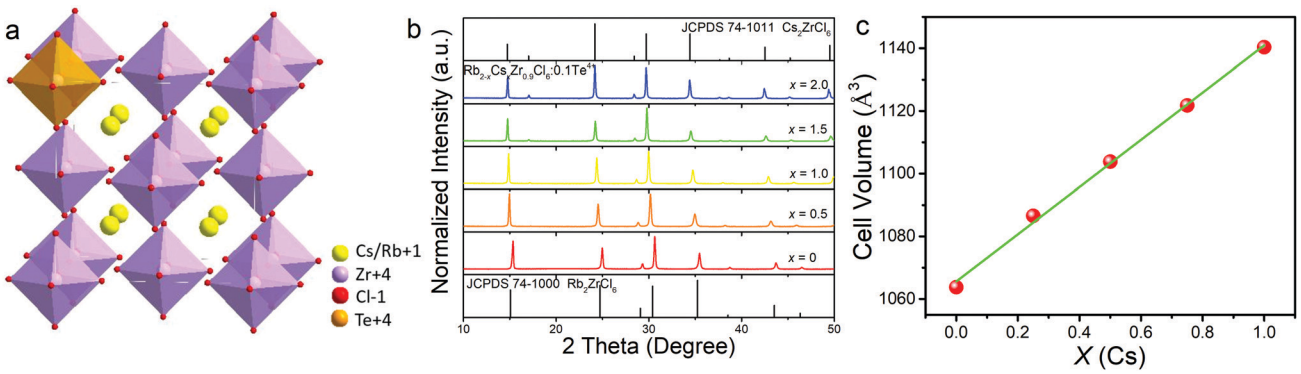

Fig. 1 (a) The crystal structure of $Rb_{2-x}Cs_xZrCl_6$:Te^{4+}. (b) XRD patterns of $Rb_{2-x}Cs_xZr_{0.9}Cl_6$:$0.1Te^{4+}$, along with JCPDS 74-1000 and JCPDS 74-1011 as a comparison. (c) The experimental cell volumes of $Rb_{2-x}Cs_xZr_{0.9}Cl_6$:$0.1Te^{4+}$ as a function of x.

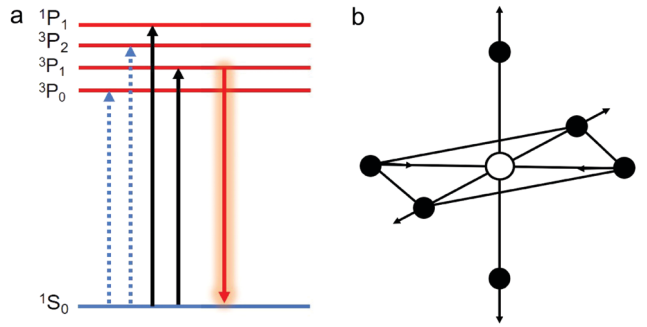

Fig. 2 (a) Schematic diagram of luminescence process for Te^{4+} in $Rb_{2-x}Cs_xZr_{0.9}Cl_6$:0.1Te^{4+}. (b) The $v2$ vibration mode of $[TeX_6]^{2-}$ octahedra.

given in Fig. 2a, which is similar to those of Bi^{3+} and Sb^{3+}.[24,25] The ground state is $^1S_0$, whereas the excited state can be split into four energy levels: singlet $^1P_1$ and triplet ^3P_n (n = 0, 1, and 2). The ^3P state undergoes spin–orbit interactions and Jahn–Teller interactions, in which the spin–orbit interactions can split ^3P into three energy levels $^3P_0$, $^3P_1$ and $^3P_2$, and the Jahn–Teller effect can also cause the ^3P state to split due to the coupling between the ^3P state and the vibrational mode.[26] According to the transition rule, the $^1S_0$–$^1P_1$ transition is allowed and the $^1S_0$–$^3P_1$ transition is partially allowed owing to a spin–orbit interaction, while the $^1S_0$–$^3P_0$ and $^1S_0$–$^3P_2$ transitions are completely forbidden at the electric dipole transition level, which can be assisted by lattice vibration. The photoluminescence in the visible light region is mainly caused by the $^3P_1$–$^1S_0$ transition.[16] For the octahedral complex MX_6 (M = s^2 and X = ligand), the vibrational modes are $v2$ and $v5$. When the luminescent center relaxes to the excited state, it shifts along the Jahn–Teller activated $v2$ and $v5$ modes. For $[TeX_6]^{2-}$ octahedra, the luminescent center shifts along the dominant $v2$ mode, and the $[TeX_6]^{2-}$ octahedra are distorted into a tetragonal shape, as shown in Fig. 2b.[26] Hence, the emission of Te^{4+} is mainly caused by self-trapped excitons (STEs), a strong Jahn–Teller distortion of the $[TeX_6]^{2-}$ octahedra.

Fig. 3a shows the absorption spectrum of $Rb_2Zr_{0.9}Cl_6$:0.1Te^{4+}, which can be divided into two absorption regions located at 300–360 nm and 380–470 nm. The shorter wavelength region is attributed to the $^1S_0$–$^3P_2$ transition, while the longer wavelength region with an asymmetric doublet comes from the $^1S_0$–$^3P_1$ transition of Te^{4+}. The doublet asymmetric phenomenon caused by the dynamic Jahn–Teller effect is common for ions with an S^2 outer electron configuration like Bi^{3+}, In^+, Sb^{3+} and Tl^+.[16,22,27,28] The wavelength-dependent PLE and PL spectra of $Rb_2Zr_{0.9}Cl_6$:0.1Te^{4+} are presented in Fig. 3b and c. Similar to the absorption spectra, the PLE spectra consist of two parts, >360 nm assigned to the $^1S_0$–$^3P_1$ transition and <360 nm assigned to the $^1S_0$–$^3P_2$ transition of Te^{4+}.[22,29] Upon excitation at 414 nm, $Rb_2Zr_{0.9}Cl_6$:0.1Te^{4+} exhibits a bright yellow emission peaked at 574 nm with a Stokes shift of 160 nm and a full width at half maximum (FWHM) of 116 nm, which is assigned to the triplet $^3P_1$–$^1S_0$ transition of Te^{4+}. Furthermore, both the wavelength-dependent PLE and

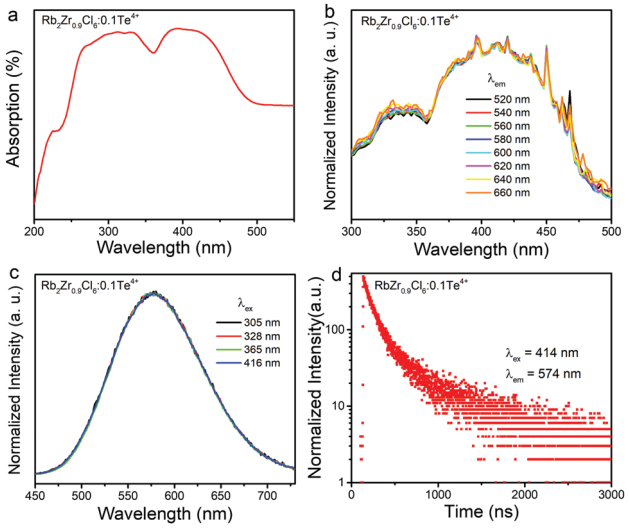

Fig. 3 (a) The absorption spectra of $Rb_2Zr_{0.9}Cl_6$:0.1Te^{4+}. Wavelength-dependent (b) PLE and (c) PL spectra of $Rb_2Zr_{0.9}Cl_6$:0.1Te^{4+}. (d) Room-temperature photoluminescence decay curve of $Rb_2Zr_{0.9}Cl_6$:0.1Te^{4+} (λ_{ex} = 414 nm and λ_{em} = 574 nm).

PL spectra show nearly no change, indicating that this yellow emission is not from surface traps or lattice defects but from the intrinsic properties of the obtained samples. In order to gain an insight into the luminous mechanism, the room-temperature decay curve of $Rb_2Zr_{0.9}Cl_6$:0.1Te^{4+} was carried out (Fig. 3d). The decay curve can be fitted well with a bi-exponential equation and the lifetime was calculated to be 235.62 μs. The broad yellow emission band, nearly unchanged wavelength-dependent PLE and PL spectra, and relatively long lifetime indicate a typical STEs emission, which is nearly consistent with those of previous reports on Te^{4+} doped phosphors.

As is reported, doping or alloying has been demonstrated to be an effective way to control the photoluminescence properties. Herein, the Cs^+ ion was used to improve the STE emission of Te^{4+} in Rb_2ZrCl_6:Te^{4+}. Fig. 4a shows the normalized absorption spectra of $Rb_{2-x}Cs_xZr_{0.9}Cl_6$:0.1Te^{4+}. With increasing concentration of Cs^+, the energy difference between the two components of the doublet bands ($^1S_0$–$^3P_1$ transition) increases, which indicates the stronger dynamical Jahn–Teller effect.[28] Fig. 4b shows the room-temperature PLE and PL spectra of $Rb_{2-x}Cs_xZr_{0.9}Cl_6$:0.1Te^{4+}. It can be seen that both the PLE and PL spectra have similar spectral profiles, except for the intensities and positions. With the introduction of Cs^+ with larger radius, the Stokes shift increases gradually from 6732.99 cm^{-1} to 6769.11 cm^{-1}, which quenches the spin–orbit interaction, promotes the Jahn–Teller distortion and improves the STE luminescence performance.[28,30,31] Hence, a significantly enhanced emission was observed in $Rb_{2-x}Cs_xZr_{0.9}Cl_6$:0.1Te^{4+}. As the PLQY is an important parameter to be considered for practical application, we measured it using an FLS920 instrument and the result is given in Table 1. For better comparison, $Cs_2Sn_{0.9}Cl_6$:0.1Te^{4+} was prepared using the same experimental conditions as $Rb_{2-x}Cs_xZr_{0.9}Cl_6$:0.1Te^{4+}. The

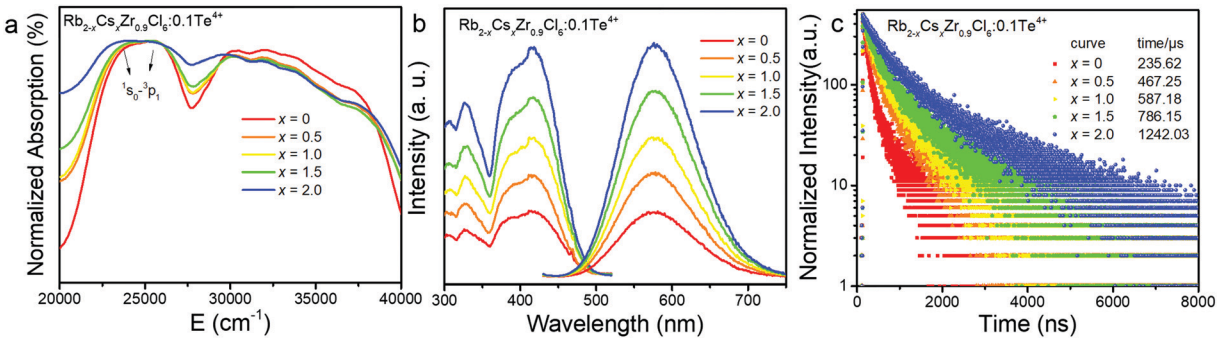

Fig. 4 (a) Room-temperature normalized absorption spectra, (b) PLE and PL spectra, and (c) decay curves of $Rb_{2-x}Cs_xZr_{0.9}Cl_6$:0.1Te^{4+}.

Table 1 The PLQY values of Te^{4+}-doped A_2BX_6 perovskite variants at room temperature

Material	Emission peak (nm)	PLQY (%)	Ref.
$Rb_2Zr_{0.97}Cl_6$:0.03Te^{4+}	574	31.78	This work
$Rb_2Zr_{0.9}Cl_6$:0.1Te^{4+}	574	20.45	This work
$Cs_2Zr_{0.97}Cl_6$:0.03Te^{4+}	579	69.73	This work
$Cs_2Zr_{0.9}Cl_6$:0.1Te^{4+}	579	41.81	This work
$Cs_2Sn_{0.95}Cl_6$:0.05Te^{4+}	573	42.3	16
$Cs_2Sn_{0.89}Te_{0.11}Cl_6$	580	95.4	17
$Cs_2Sn_{0.9}Cl_6$:0.1Te^{4+}	580	52.07	This work

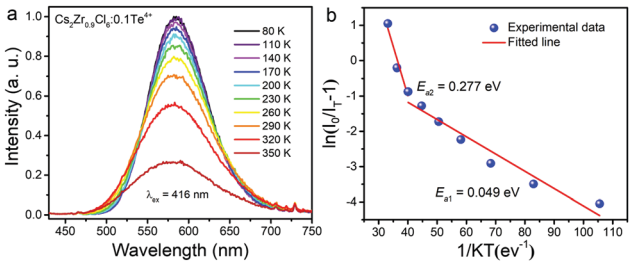

Fig. 5 (a) Temperature-dependent PL spectra of $Cs_2Zr_{0.9}Cl_6$:0.1Te^{4+} and (b) plot of $\ln(I_0/I_T - 1)$ *versus* $1/kT$ of the $Cs_2Zr_{0.9}Cl_6$:0.1Te^{4+} phosphor.

relatively high PLQY indicates that Cs_2ZrCl_6:Te^{4+} has great application potential in the field of solid-state lighting. On the other hand, a slight red-shift of the emission spectrum is observed, which is due to the expansion of Te-anion bonds and strain variation of the [$TeCl_6$] octahedron.[16,32] The decay curves of $Rb_{2-x}Cs_xZr_{0.9}Cl_6$:0.1Te^{4+} are presented in Fig. 4c. It was observed that the lifetime values of Te^{4+} tend to increase with the increasing content of Cs^+ ions, demonstrating that radiative transition is enhanced in $Rb_{2-x}Cs_xZr_{0.9}Cl_6$:0.1Te^{4+}.[33] Therefore, Cs_2ZrCl_6:Te^{4+} was selected as the studied composition of the potential yellow-emitting phosphors for solid-state lighting field in the present series.

Temperature is a vital parameter affecting the luminescence properties. Fig. 5a presents the temperature-dependent PL spectra of $Cs_2Zr_{0.9}Cl_6$:0.1Te^{4+}. With an increase in temperature, the shape of the PL spectra remains basically unchanged, demonstrating no phase transition in this temperature range. On the other hand, the PL quenching temperature of this $Cs_2Zr_{0.9}Cl_6$:0.1Te^{4+} is up to 350 K, superior to those of other A_2BX_6 perovskite variants such as Cs_2SnCl_6:Bi^{3+}, $Cs_2Sn_{1-x}Te_xCl_6$ and $Cs_2Hf(Cl/Br)_6$:1%Te.[17,24,34] The temperature dependence of the phosphor can be expressed by the Arrhenius formula:[35]

$$I(T) = \frac{I_0}{1 + A\exp\left(-\frac{E_a}{kT}\right)} \quad (1)$$

where I_0 is the initial PL intensity, I_T is the PL intensity at different temperatures, A is a constant, k is the Boltzmann constant (8.62×10^{-5} eV), and E_a is the activation energy for thermal quenching. Usually, a larger activation energy E_a will cause a lower probability of non-radiation, while a lower activation energy E_a will lead to severe thermal quenching behavior.[36] According to this equation, two E_a values were observed, 0.277 eV (E_{a2}) at a high temperature and 0.049 eV (E_{a1}) at a low temperature, which indicate that two thermal processes occurred in $Cs_2Zr_{0.9}Cl_6$:0.1Te^{4+} (Fig. 5b). E_{a1} is a thermal quenching phenomenon caused by nonradiative transitions at the intersection of excited and ground states. Hence, the high-temperature process should be a thermal ionization process and the temperature dependence of the multiple thermal processes can be expressed using the following formula:[37]

$$I(T) = \frac{I_0}{1 + A_1\exp\left(-\frac{E_{a1}}{kT}\right) + A_2\exp\left(-\frac{E_{a2}}{kT}\right)} \quad (2)$$

Stability and application

Considering the stability of luminescent materials is another crucial parameter for their future applications, their thermal and anti-water stability of $Cs_2Zr_{0.9}Cl_6$:0.1Te^{4+} has been thoroughly investigated. We firstly carried out TGA analysis of the as-prepared $Cs_2Zr_{0.9}Cl_6$:0.1Te^{4+}. As shown in Fig. 6a, the sample retains a weight of 95% at 595 °C, which demonstrates good thermal stability. Besides, the powder was put into a cuvette with deionized water to measure the luminescence and structural stability against water. $Cs_2Zr_{0.9}Cl_6$:0.1Te^{4+} exhibits strong yellow emission under 416 nm excitation after 330 min soaking in deionized water (Fig. 6b). XRD characterization implies no

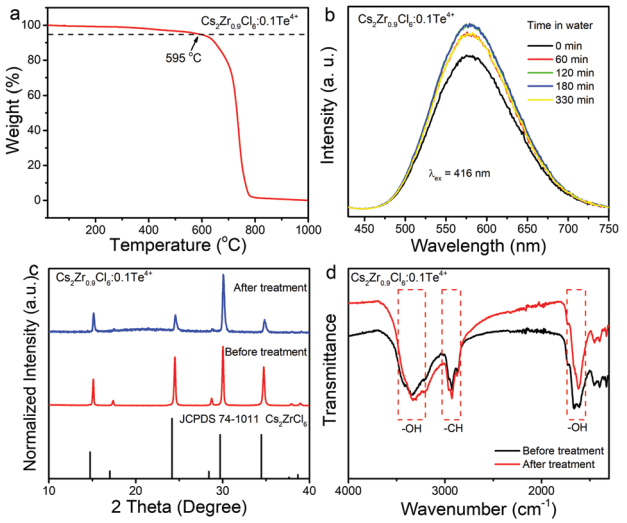

Fig. 6 (a) TGA data of as-synthesized $Cs_2Zr_{0.9}Cl_6$:0.1Te^{4+}. (b) PL stability of $Cs_2Zr_{0.9}Cl_6$:0.1Te^{4+} after immersion into deionized water for different durations. (c) XRD patterns and (d) FT-IR of the sample before and after treatment.

detectable impurity of hydrated products such as CsCl, $ZrCl_4$ and ZrO_2 (Fig. 6c). Moreover, the FT-IR result shows that no other new vibration signals appeared (Fig. 6d). Hence, we suspected that this good anti-water stability is possibly attributed to the formation of an amorphous alteration phase, which is similar to Cs_2SnCl_6 and $Cs_2Sn_{1-x}Te_xCl_6$.[17,38]

The high PLQY, and good thermal and anti-water stability endow $Cs_2Zr_{0.97}Cl_6$:0.03Te^{4+} with highly promising prospects in solid state lighting. Hence, we constructed white light-emitting diodes (WLEDs) by combining our $Cs_2Zr_{0.97}Cl_6$:0.03Te^{4+} sample, the commercial blue phosphor $BaMgAl_{10}O_{17}$:Eu^{2+} (BAM:Eu^{2+}) and NUV LED InGAN chips (λ_{ex} = 395 nm). Fig. 7a shows the PL spectra of the WLED devices at a current of 20 mA. The CIE color coordinate is (0.3407, 0.3561) related to a warm white correlated color temperature (CCT) of 5182 K and a color rendering index (CRI, R_a) of 79. The above results indicate that $Cs_2Zr_{0.97}Cl_6$:0.03Te^{4+} could be considered as an excellent candidate in the field of NUV WLEDs.

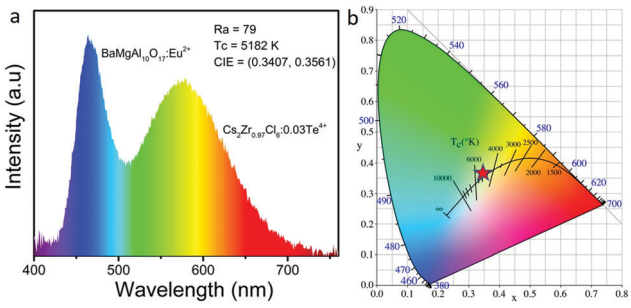

Fig. 7 (a) PL spectra of WLEDs fabricated using our phosphor $Cs_2Zr_{0.97}Cl_6$:0.03Te^{4+} and commercial blue phosphor BAM:Eu^{2+} on 395 nm InGAN chips at 20 mA drive current. (b) CIE chromaticity diagram of $Cs_2Zr_{0.97}Cl_6$:0.03Te^{4+} of the fabricated WLED.

Conclusions

In summary, we synthesized a series of $Rb_{2-x}Cs_xZrCl_6$:Te^{4+} lead-free perovskite variants with a yellow emission attributed to the Jahn–Teller like STEs. By gradual substitution of Rb^+ with Cs^+, the cubic lattice constants of the solid solutions increase linearly and the emission enhance greatly by the stronger Jahn–Teller distortion. Thanks to the high PLQY and excellent thermal and water stability of Cs_2ZrCl_6:Te^{4+}, we constructed a warm WLED by combining this yellow phosphor with a commercial blue phosphor and 395 nm LED chip. Such success in $Rb_{2-x}Cs_xZrCl_6$:Te^{4+} will open up new avenues for the development of novel lead-free perovskite variants for emerging optoelectronic applications.

Conflicts of interest

There are no conflicts to declare.

Acknowledgements

This work is supported by Beijing Natural Science Foundation (No. 2214068), the National Natural Science Foundation of China (No. 61705003), and the Beijing Technology and Business University Research Team Construction Project (No. PXM2019_014213_000007 and PXM2020_014213_000017).

Notes and references

1 J. S. Manser, J. A. Christians and P. V. Kamat, Intriguing Optoelectronic Properties of Metal Halide Perovskites, *Chem. Rev.*, 2016, **116**, 12956–13008.
2 J. Z. Song, J. H. Li, X. M. Li, L. M. Xu, Y. H. Dong and H. B. Zeng, Quantum Dot Light-Emitting Diodes Based on Inorganic Perovskite Cesium Lead Halides $CsPbX_3$, *Adv. Mater.*, 2015, **27**, 7162–7167.
3 J. Liang, Z. H. Liu, L. B. Qiu, Z. Hawash, L. Q. Meng, Z. F. Wu, Y. Jiang, L. K. Ono and Y. B. Qi, Enhancing Optical, Electronic, Crystalline, and Morphological Properties of Cesium Lead Halide by Mn Substitution for High-Stability All-Inorganic Perovskite Solar Cells with Carbon Electrodes, *Adv. Energy Mater.*, 2018, 8.
4 C. X. Bao, J. Yang, S. Bai, W. D. Xu, Z. B. Yan, Q. Y. Xu, J. M. Liu, W. J. Zhang and F. Gao, High Performance and Stable All-Inorganic Metal Halide Perovskite-Based Photodetectors for Optical Communication Applications, *Adv. Mater.*, 2018, **30**, 1803422.
5 J. J. Luo, S. R. Li, H. D. Wu, Y. Zhou, Y. Li, J. Liu, J. H. Li, K. H. Li, F. Yi, G. D. Niu and J. Tang, Cs_2AgInC_{l6} Double Perovskite Single Crystals: Parity Forbidden Transitions and Their Application For Sensitive and Fast UV Photodetectors, *ACS Photonics*, 2017, **5**, 398–405.
6 J. J. Luo, M. C. Hu, G. D. Niu and J. Tang, Lead-Free Halide Perovskites and Perovskite Variants as Phosphors toward Light-Emitting Applications, *ACS Appl. Mater. Interfaces*, 2019, **11**, 31575–31584.

7 C. C. Stoumpos, L. Frazer, D. J. Clark, Y. S. Kim, S. H. Rhim, A. J. Freeman, J. B. Ketterson, J. I. Jang and M. G. Kanatzidis, Hybrid germanium iodide perovskite semiconductors: active lone pairs, structural distortions, direct and indirect energy gaps, and strong nonlinear optical properties, *J. Am. Chem. Soc.*, 2015, **137**, 6804–6819.

8 J. Zhou, J. J. Luo, X. M. Rong, P. J. Wei, M. S. Molokeev, Y. Huang, J. Zhao, Q. L. Liu, X. W. Zhang, J. Tang and Z. G. Xia, Lead-Free Perovskite Derivative $Cs_2SnCl_{6-x}Br_x$ Single Crystals for Narrowband Photodetectors, *Adv. Opt. Mater.*, 2019, 7.

9 A. Kaltzoglou, M. Antoniadou, A. G. Kontos, C. C. Stoumpos, D. Perganti, E. Siranidi, V. Raptis, K. Trohidou, V. Psycharis, M. G. Kanatzidis and P. Falaras, Optical-Vibrational Properties of the Cs_2SnX_6 (X = Cl, Br, I) Defect Perovskites and Hole-Transport Efficiency in Dye-Sensitized Solar Cells, *J. Phys. Chem. C*, 2016, **120**, 11777–11785.

10 B. Lee, C. C. Stoumpos, N. Zhou, F. Hao, C. Malliakas, C. Y. Yeh, T. J. Marks, M. G. Kanatzidis and R. P. Chang, Air-stable molecular semiconducting iodosalts for solar cell applications: Cs_2SnI_6 as a hole conductor, *J. Am. Chem. Soc.*, 2014, **136**, 15379–15385.

11 J. J. Luo, X. M. Wang, S. R. Li, J. Liu, Y. M. Guo, G. D. Niu, L. Yao, Y. H. Fu, L. Gao, Q. S. Dong, C. Y. Zhao, M. Y. Leng, F. S. Ma, W. X. Liang, L. D. Wang, S. Y. Jin, J. B. Han, L. J. Zhang, J. Etheridge, J. B. Wang, Y. F. Yan, E. H. Sargent and J. Tang, Efficient and stable emission of warm-white light from lead-free halide double perovskites, *Nature*, 2018, **563**, 541–545.

12 B. Ke, R. S. Zeng, Z. Zhao, Q. L. Wei, X. G. Xue, K. Bai, C. X. Cai, W. C. Zhou, Z. G. Xia and B. S. Zou, Homo- and Heterovalent Doping-Mediated Self-Trapped Exciton Emission and Energy Transfer in Mn-Doped $Cs_2Na_{1-x}Ag_xBiCl_6$ Double Perovskites, *J. Phys. Chem. Lett.*, 2020, **11**, 340–348.

13 Y. Liu, X. M. Rong, M. Li, M. S. Molokeev, J. Zhao and Z. G. Xia, Incorporating Rare-Earth Terbium(III) Ions into $Cs_2AgInCl_6$:Bi Nanocrystals toward Tunable Photoluminescence, *Angew. Chem., Int. Ed.*, 2020, **59**, 11634–11640.

14 Y. Y. Jing, Y. Liu, J. Zhao and Z. G. Xia, Sb^{3+} Doping-Induced Triplet Self-Trapped Excitons Emission in Lead-Free Cs_2SnCl_6 Nanocrystals, *J. Phys. Chem. Lett.*, 2019, **10**, 7439–7444.

15 C. Y. Wang, P. Liang, R. J. Xie, Y. Yao, P. Liu, Y. T. Yang, J. Hu, L. Y. Shao, X. W. Sun, F. Y. Kang and G. D. Wei, Highly Efficient Lead-Free (Bi,Ce)-Codoped $Cs_2Ag_{0.4}Na_{0.6}InCl_6$ Double Perovskites for White Light-Emitting Diodes, *Chem. Mater.*, 2020, **32**, 7814–7821.

16 R. S. Zeng, K. Bai, Q. L. Wei, T. Chang, J. Yan, B. Ke, J. L. Huang, L. S. Wang, W. C. Zhou, S. Cao, J. L. Zhao and B. S. Zou, Boosting triplet self-trapped exciton emission in Te(IV)-doped Cs_2SnCl_6 perovskite variants, *Nano Res.*, 2021, **14**, 1551–1558.

17 Z. F. Tan, Y. M. Chu, J. X. Chen, J. H. Li, G. Q. Ji, G. D. Niu, L. Gao, Z. W. Xiao and J. Tang, Lead-Free Perovskite Variant Solid Solutions $Cs_2Sn_{1-x}Te_xCl_6$: Bright Luminescence and High Anti-Water Stability, *Adv. Mater.*, 2020, **32**, 2002443.

18 P. J. H. Drummen, H. Donker, W. M. A. Smit and G. Blasse, Jahn-Teller distortion in the excited state of tellurium (IV) in Cs_2MCl_6 (M = Zr, Sn), *Chem. Phys. Lett.*, 1988, **144**, 460–462.

19 R. Wernicke, H. Kupka, W. Ensslin and H. H. Schmidtke, Low temperature luminescence spectra of the $d^{10}s^2$ complexes Cs_2MX_6 (M = Se, Te and X = Cl, Br), *Chem. Phys.*, 1980, **47**, 235–244.

20 F. Li, S. Huang, X. Y. Liu, Z. L. Bai, Z. T. Wang, H. D. Xie, X. D. Bai and H. Z. Zhong, Highly Stable and Spectrally Tunable Gamma Phase $Rb_xCs_{1-x}PbI_3$ Gradient-Alloyed Quantum Dots in PMMA Matrix through A Sites Engineering, *Adv. Funct. Mater.*, 2021, **31**, 2008211.

21 B. M. Benin, D. N. Dirin, V. Morad, M. Worle, S. Yakunin, G. Raino, O. Nazarenko, M. Fischer, I. Infante and M. V. Kovalenko, Highly Emissive Self-Trapped Excitons in Fully Inorganic Zero-Dimensional Tin Halides, *Angew. Chem., Int. Ed.*, 2018, **57**, 11329–11333.

22 C. Tong, Q. L. Wei, R. S. Zeng, S. Cao, J. L. Zhao and B. S. Zou, Efficient Energy Transfer in Te^{4+}-Doped Cs_2ZrCl_6 Vacancy-Ordered Perovskites and Ultrahigh Moisture Stability *via* A-Site Rb-Alloying Strategy, *J. Phys. Chem. Lett.*, 2021, **12**, 1829–1837.

23 *TOPAS: General profile and structure analysis software for powder diffraction data, VERSION 4; Bruker AXS*, Karlsruhe, German, 2008.

24 Z. F. Tan, J. H. Li, C. Zhang, Z. Li, Q. S. Hu, Z. W. Xiao, T. Kamiya, H. Hosono, G. D. Niu, E. Lifshitz, Y. B. Cheng and J. Tang, Highly Efficient Blue-Emitting Bi-Doped Cs_2SnCl_6 Perovskite Variant: Photoluminescence Induced by Impurity Doping, *Adv. Funct. Mater.*, 2018, **28**, 1801131.

25 J. H. Li, Z. F. Tan, M. C. Hu, C. Chen, J. J. Luo, S. R. Li, L. Gao, Z. W. Xiao, G. D. Niu and J. Tang, Antimony doped Cs_2SnCl_6 with bright and stable emission, *Front. Optoelectron.*, 2019, **12**, 352–364.

26 J. Y. Sun, H. Y. Du and W. X. Hu, *Solid luminescent materials*, Chemical Industry Press, Beijing, 2003.

27 H. Cai, Z. Song and Q. L. Liu, Infrared-photostimulable and long-persistent ultraviolet-emitting phosphor $LiLuGeO_4$:-Bi^{3+},Yb^{3+} for biophotonic applications, *Mater. Chem. Front.*, 2021, **5**, 1468–1476.

28 E. W. J. L. Oomen, W. M. A. Smit and G. Blasse, Jahn-Teller effect in the emission and excitation spectra of the Sb^{3+} ion in LPO_4 (L = Sc, Lu, Y), *Phys. Rev. B: Condens. Matter Mater. Phys.*, 1988, **37**, 18–26.

29 T. V. Sedakova and A. G. Mirochnik, Luminescent and thermochromic properties of tellurium(IV) halide complexes with cesium, *Opt. Spectrosc.*, 2016, **120**, 268–273.

30 S. Masunaga, N. Goto, A. Matsushima and A. Fukuda, Hydrostatic Pressure Effects on the Triplet Relaxed Excited States of KI: Tl^+-Type Phosphors through the Quadratic Jahn-Teller Interaction, *J. Phys. Soc. Jpn.*, 1977, **43**, 2013–2020.

31 D. Mugnai, A. Ranfagni, O. Pilla, G. Viliani and M. Montagna, Trap depth in Tl^+-like phosphors: Deduction of Jahn-Teller coupling constants, *Solid State Commun.*, 1980, **35**, 975–977.

32 B. M. Benin, D. N. Dirin, V. Morad, M. Worle, S. Yakunin, G. Raino, O. Nazarenko, M. Fischer, I. Infante and M. V. Kovalenko, Highly Emissive Self-Trapped Excitons in Fully Inorganic Zero-Dimensional Tin Halides, *Angew. Chem., Int. Ed.*, 2018, **57**, 11329–11333.

33 J. Zhou, M. Z. Li, M. S. Molokeev, J. Y. Sun, D. H. Xu and Z. G. Xia, Tunable photoluminescence in Sb^{3+}-doped zero-dimensional hybrid metal halides with intrinsic and extrinsic self-trapped excitons, *J. Mater. Chem. C*, 2020, **8**, 5058–5063.

34 Y. Fujimoto, K. Saeki, D. Nakauchi, H. Fukada, T. Yanagida, H. Kawamoto, M. Koshimizu and K. Asai, Photoluminescence, photoacoustic, and scintillation properties of Te^{4+}-doped Cs_2HfCl_6 crystals, *Mater. Res. Bull.*, 2018, **105**, 291–295.

35 X. Y. Ji, J. L. Zhang, Y. Li, S. Z. Liao, X. G. Zhang, Z. Y. Yang, Z. L. Wang, Z. X. Qiu, W. L. Zhou, L. P. Yu and S. X. Lian, Improving Quantum Efficiency and Thermal Stability in Blue-Emitting $Ba_{2-x}Sr_xSiO_4$:Ce^{3+} Phosphor *via* Solid Solution, *Chem. Mater.*, 2018, **30**, 5137–5147.

36 B. Bai, P. P. Dang, D. Y. Huang, H. Z. Lian and J. Lin, Broadband Near-Infrared Emitting $Ca_2LuScGa_2Ge_2O_{12}$:Cr^{3+} Phosphors: Luminescence Properties and Application in Light-Emitting Diodes, *Inorg. Chem.*, 2020, **59**, 13481–13488.

37 Q. Q. Zhu, L. Wang, N. Hirosaki, L. Y. Hao, X. Xu and R. J. Xie, Extra-Broad Band Orange-Emitting Ce^{3+}-Doped $Y_3Si_5N_9O$ Phosphor for Solid-State Lighting: Electronic, Crystal Structures and Luminescence Properties, *Chem. Mater.*, 2016, **28**, 4829–4839.

38 W. G. Zhu, T. K. Yao, J. H. Shen, W. Q. Xu, B. W. Gong, Y. C. Wang and J. Lian, In situ Investigation of Water Interaction with Lead-Free All Inorganic Perovskite ($Cs_2SnI_xCl_{6-x}$), *J. Phys. Chem. C*, 2019, **123**, 9575–9581.